Real-Time Imaging **1**, 95–104 (1995)

Mammographic Computer-Assisted Diagnosis using Computational Statistics Pattern Recognition

Research begun for target identification utilizing pattern recognition has been applied to mammographic computer-assisted diagnosis. The research has utilized the discipline of computational statistics. Feature extraction based on fractals and incorporating segmentation boundaries led to probability density estimation and classification based on discriminant analysis. The results of applying these techniques to mammography are very promising and are reported herein. The results of these limited mammographic studies are discussed in their own light and in comparison with other's work.

R.A. Lorey, J.L. Solka, G.W. Rogers, D.J. Marchette and C.E. Priebe

Advanced Computation Technology Group, Naval Surface Warfare Center, Dahlgren Division, Dahlgren, VA 22448 and Department of Mathematical Sciences, The Johns Hopkins University, Baltimore, MD 21218 USA. Email: rlorey@relay.nswc.navy.mil

Introduction

The issue of locating and identifying potential targets has historically posed problems in war-fighting scenarios. Modern warfare, with its rapid deployment, quick strike capability, and smart weapons usage has exacerbated this situation as evident in Desert Storm. Future war-making capabilities with its need for faster, or even on the fly, mission planning will exceed the limits of today's technology for target identification. It is in this light that the research, sponsored by the Office of Naval Research, was undertaken at the Naval Surface Warfare Center, Dahlgren Division (NSWCDD).

The technology necessary to identify man-made objects as distinct from natural objects is the same technology that can be used to identify any class of object. Thus, with the advent of Technology Transfer it was natural for NSWCDD to apply its expertise to other areas. The Research Triangle Institute and the Federal Laboratory Consortium Demonstration Project on Critical Industry Needs opened the door for this application. Specifically, the August 1992 National Cancer Institute problem statement called for software for computer-assisted diagnosis (CAD), image processing, and pattern recognition for use in digital mammography systems. It is in this light that our research has been directed toward application of this technology to mammographic CAD. Successful efforts in this endeavor, potentially a more difficult pattern recognition problem, could well result in further advances in the state-of-the-art.

Computational Statistics Pattern Recognition

Our method for solving the pattern recognition problem involves the use of Computational Statistics (1).

1077-2014/95/020095 + 10 $08.00/0

This theory involves very large datasets and does not incorporate assumptions about the parametric behaviour of the data. Seemingly intractable problems can sometimes yield to these techniques.

Here, we consider gray scale digital images. Each class of object in the image is characterized by a pattern or texture. We wish to analyse images and determine where changes in the pattern or texture (class) occur. Such detections enable us to distinguish targets from non-targets, man-made from natural objects, or tumours from healthy tissue.

Features

We are concerned with local texture features. We wish to categorize the features belonging to a given pattern in order to sort them into various classes. This is done by deriving features using the theory of fractal dimension (2). The fractal dimension 'D' (as distinguished from the normal Euclidean dimension 'd') can be estimated using Richardson's Power Law (2).

$$M(\varepsilon) = K\,\varepsilon^{(d-D)}, \qquad [1]$$

where $M(\varepsilon)$ is the measured property of a fractal at a scale ε and K is a proportionality constant. This equation and the technique described in Solka *et al.* (3) allows us to extract three features that describe the texture. Thus, in a digitized image each pixel can be characterized by a 3-D feature vector $\vec{x} = [x_1,x_2,x_3]^t$ based on a small neighbourhood of the principal pixel. One feature is directly related to the fractal dimension, one is a measure of how well the fractal model fits the data, and one is related to the local degree of contrast in an image. Further, from a single image, M, we have available a large sample of observations $X_M = [\vec{x}_1^t,\ldots,\vec{x}_{n_m}^t]^t$. Using these features we construct probability density functions for different classes and use these for discrimination.

Probability Density Estimation

The types of problems amenable to these techniques are not those whose probability density function (pdf) can be represented by usual statistical models (e.g. normal distributions). A digitized image can easily represent a dataset of up to 10^7 local observations and our work indicates this data is not well represented by a normal distribution. We estimate the pdf using a technique such as adaptive mixtures (4–6). It is a hybrid approach which maintains the best features of the kernel estimation model (7) and the finite mixture model (8) and does not make strict assumptions about the data distribution. The general mixture density can be given by,

$$\hat{\alpha}(x;\theta,\pi) = \int_{\Omega}\phi(x|\theta)\,dF_{\pi}(\theta), \qquad [2]$$

where $\hat{\alpha}(x))$ is the estimate for the true pdf $\alpha(x)$ underlying the sample X_M, ϕ is a fixed known function and F is the mixing distribution.

Segmentation Boundaries

As described by Priebe *et al.* (9), we can incorporate segmentation boundaries into the calculation of the fractal dimension features and hence into the pdf. Incorporation of segmentation boundaries provides for significantly more discriminatory information in the texture features and the associated pdfs. This reference further describes the two texture patches from Brodatz (10) shown in Figure 1. Although this may seem to be a trivial case, it is illustrative of the technique. The three regions shown in Figure 1 (numbered 1–3 from the left) shows a pure texture (D17 from Brodatz) in 1 and a pure texture (D24 of Brodatz) in 3. Region 2 straddles the boundary between the two textures. Figure 2 shows the results of a pdf calculation (single feature) of the regions of Figure 1. α_1 and α_3 are the pdfs of regions 1 and 3, respectively. The two plots of α_2 (region 2) shows the effect of incorporating or not incorporating the boundary. Clearly, incorporating the boundary gives a truer picture of the pdf of the region.

Computational Complexity Reduction

For each observation the extracted fractal features are represented by $\vec{x} = [x_1,x_2,x_3]^t$. While it is true that more information is often contained in higher dimensional feature space, the computational complexity increases dramatically with any increase in the dimension (11). To reduce this complexity and simplify the computations, we use the Fisher Linear Discriminant (FLD) (12). The FLD projects the three dimensions to the one dimension that is in some sense best for discrimination. The method and results have been described in Priebe *et al.* (13). As shown there, using all three features and the FLD yields better correlation with class than any single feature alone.

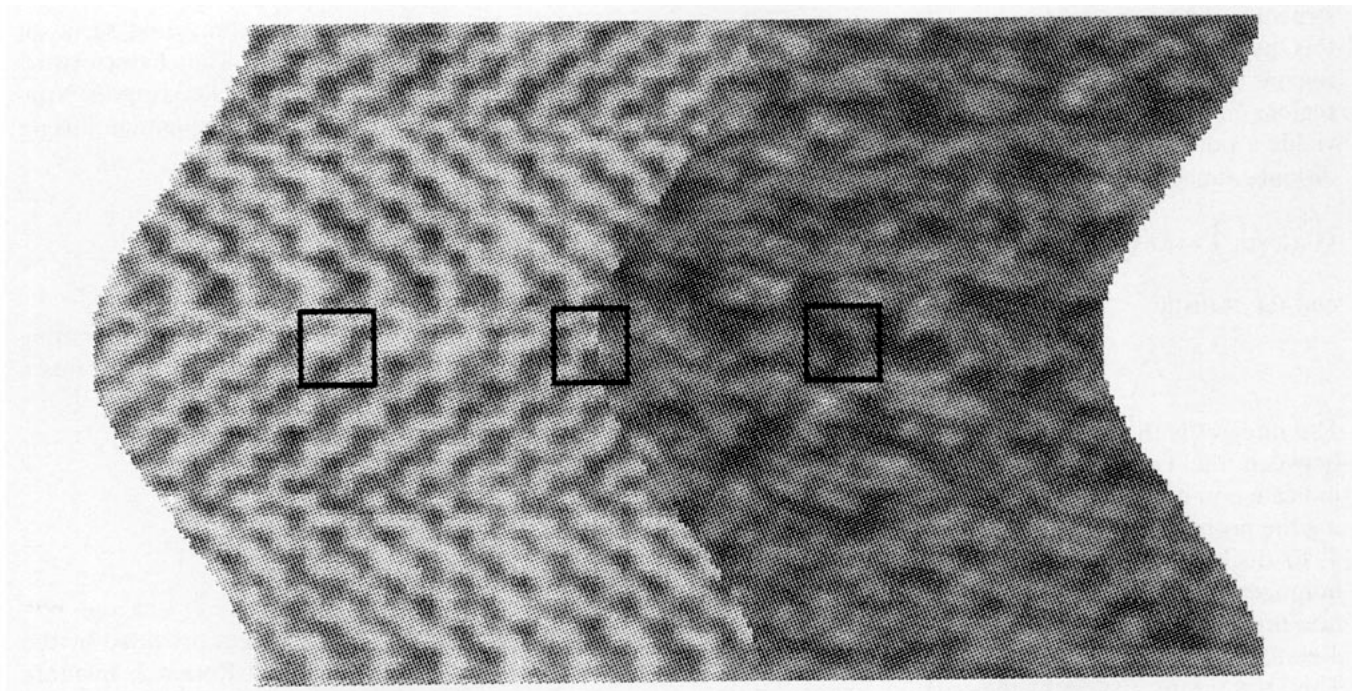

Figure 1. Two adjacent texture patches and three regions numbered 1–3 from the left.

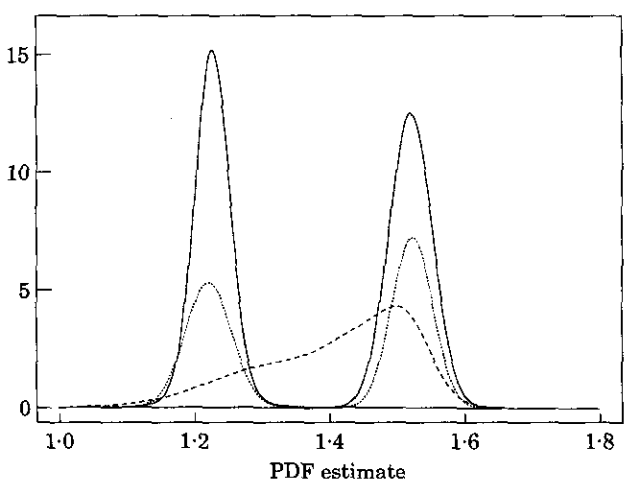

Figure 2. Single feature probability density functions for the three regions from Figure 1

Discriminant Analysis

The probability density function characteristics are used to discriminate among the classes (14,15) by a relatively straightforward application of Bayes' rule (12). Here we consider

$$X_M = \bigcup_{\alpha \varepsilon A_M} X_{M_\alpha}, \qquad [3]$$

where A_M is a set of one or more classes. That is, observations from each image may be drawn from more than one class. In the simplest case, $A_M = \{1,2\}$. Hence, with estimates $\hat{\alpha}_1$ and $\hat{\alpha}_2$ for two classes based on observations X_{M_1} and X_{M_2} (from image M), the likelihood ratio test statistic, $LR(\zeta) = \hat{\alpha}(\zeta)/\hat{\alpha}(\zeta)$, is used to indicate the proper classification for the observation ζ drawn from another image. Generalization issues of utilizing estimates from observations from one image for discriminating classes in another image need to be addressed (16). At a minimum, to discriminate classes in image k (classify the observations in X_M^k) a large number of training observations from images X_M^i ($i = 1,..., p; i \neq k$) will need to be used to build the estimates $\hat{\alpha}_1$ and $\hat{\alpha}_2$ for the two classes.

Change Point Analysis

Spatial Change Points

With the assumption that an image consists of observations from more than one class, another approach is to investigate the homogeneity of the texture. Considering whether or not the probabilistic structure of an image is uniform throughout may be construed as a spatial change point detection problem (17). The hypothesis is that there is a region in an image whose probabilistic

structure differs from the norm. The investigation of this hypothesis begins by considering small sample regions, $Y_{M_i} \subset X_M$, i = 1, ..., M. These small sample regions may or may not intersect. Each small sample yields a pdf estimate $\hat{\alpha}_{M_i}$. From these, we can form a distance function

$$f\left(\hat{\alpha}_{M_i}, \hat{\alpha}_{M_j}\right) = KL\left(\hat{\alpha}_{M_i}, \hat{\alpha}_{M_j}\right) = \int \hat{\alpha}_{M_i} \bullet \log\left(\hat{\alpha}_{M_i} / \hat{\alpha}_{M_j}\right), \quad (4)$$

and the statistic

$$T = \sup_{i,j} f\left(\hat{\alpha}_{M_i}, \hat{\alpha}_{M_j}\right). \quad (5)$$

The integral is the Kullback-Liebler (KL) information between the two distributions and can be used to indicate non-homogeneity (16). This is done by estimating the probability density of the KL statistic and using T to distinguish between the homogeneous or non-homogeneous class. T greater than some τ indicates non-homogeneity and estimating the distribution of the T statistic allows a computation of an empirical p-value. This procedure fits into the spatial change point detection framework when each Y_{M_i} is considered to be a spatially connected region. An appropriate value of τ is determined through training, that is, we wish to determine the relationship between T values and the likelihood that an observation deviation indicates non-homogeneity.

Spatio-temporal Change Points

This technique is also useful for detecting changes over time. We can consider images of the same scene or object produced at different times. The characteristics of the regions of the images are modelled by pdfs. Non-homogeneity in a like region of sequential images indicates a spatio-temporal change point.

Proposed CAD System

Figure 3 shows a proposed system (18) incorporating the items discussed above. This flowchart represents a very high level schematic.

Experimental Results

Mammographic pdfs

We conducted this study using images provided by the H. Lee Moffitt Cancer Center and Research Institute and the Department of Radiology of the University of South Florida (13). All tumourous regions were biopsy proven. The mammograms were digitized at approximately 220 μm per pixel and 8 bits per pixel. Figure 4 shows regions of healthy and tumorous (approximately 10 mm malignant stellate mass) tissue from a mammogram A. Ten thousand healthy tissue observations and 500 tumorous tissue observations were used for training data. Mammogram B (not pictured) containing an approximately 6 mm malignant stellate mass was used

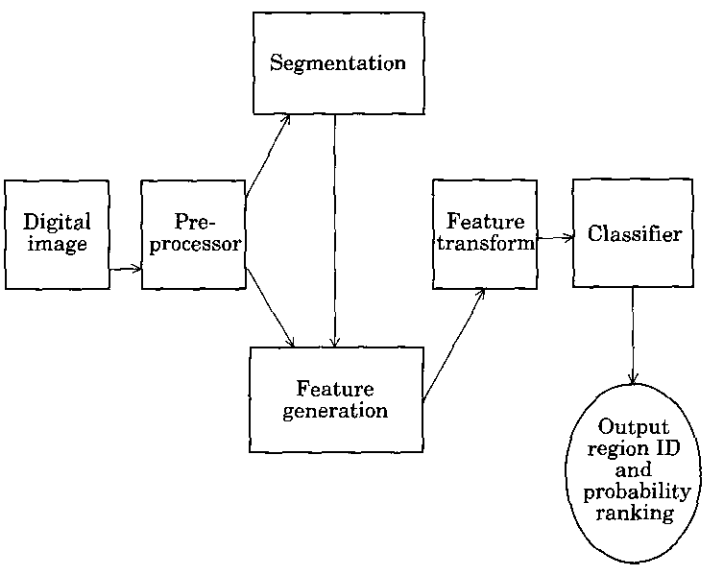

Figure 3. Proposed computer-assisted diagnosis system flowchart.

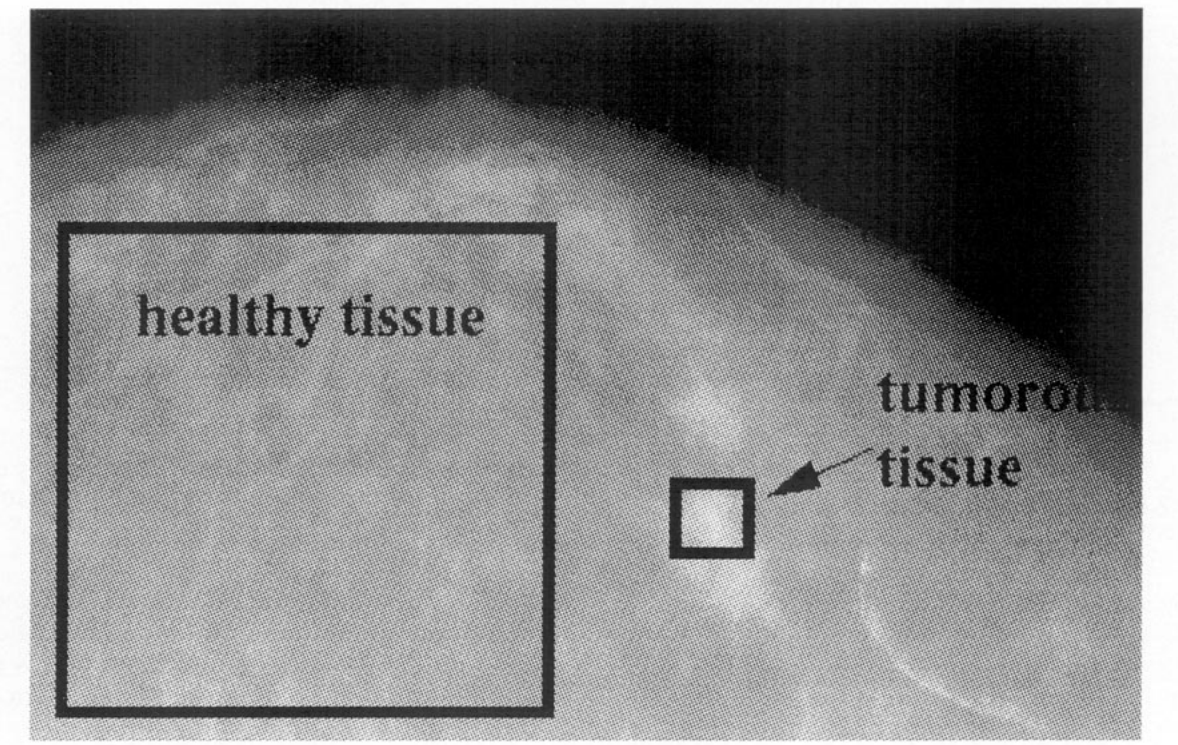

Figure 4. Regions of interest in mammogram A. This image has been enhanced for presentation.

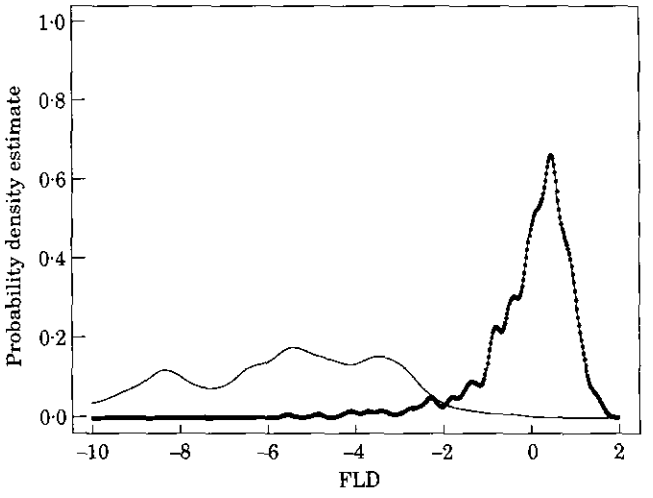

Figure 5. Fisher Linear discriminant (FLD) probability density functions for mammogram A. (—), Tumour; (—), healthy.

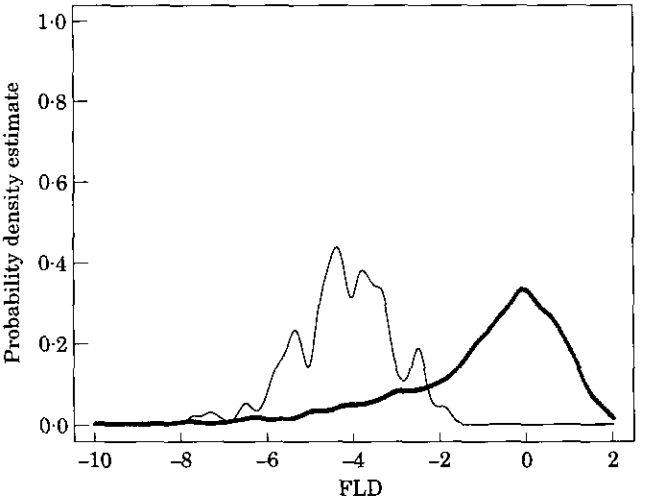

Figure 6. Fisher Linear discriminant (FLD) probability density functions for mammogram B using the independent projection. (—), Tumour; (—), healthy.

for testing (10 000 healthy tissue observations and 300 tumorous tissue observations).

Figure 5 is a plot of the pdfs of the projected data showing the separation of the healthy and tumorous classes for mammogram A. The FLD and transformation from A is applied to B and the results are shown in Figure 6. The discriminant boundary is clearly evident and appears to be invariant. When the roles of A and B are reversed, the plots exhibit the same behaviour but with a different discriminant boundary. Based on this

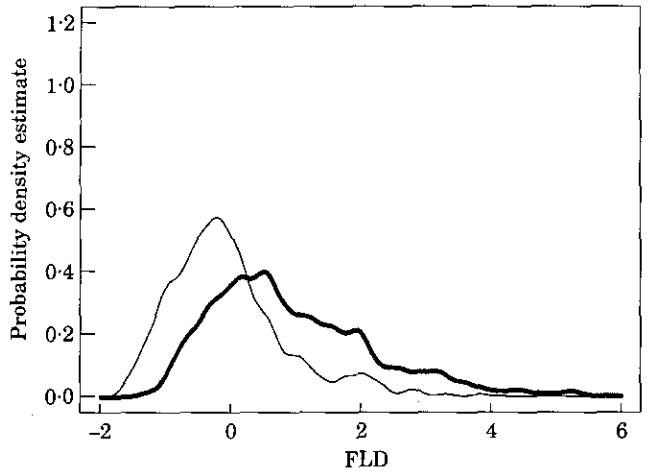

Figure 7. Fisher linear discriminant probability density functions for mammogram N1 (—) vs. mammogram DY (—).

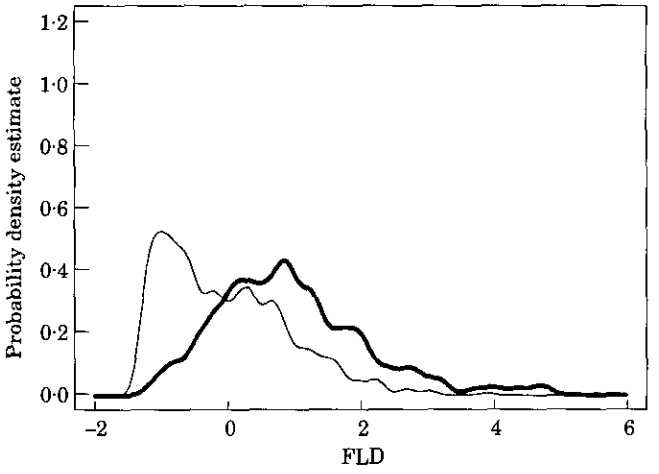

Figure 8. Fisher linear discriminant(FLD) probability density functions for mammogram N1 (—) vs. mammogram P1 (—).

limited study, the results indicate the possibility that once a projection is chosen the discriminant boundary is invariant from training to testing data. Thus a discriminant boundary obtained from training images can be successfully applied to new test images.

Wolfe's Patterns

Wolfe distinguished four tissue patterns (labelled as N1, P1, P2 and DY) corresponding to increasing breast tissue density and different morphology (19). To determine the applicability of this technique to the discrimination of Wolfe patterns, we analysed an additional

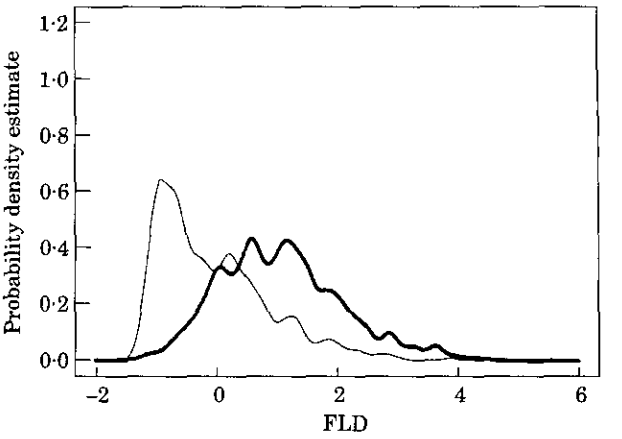

Figure 9. Fisher linear discriminant (FLD) probability density functions for mammogram N1 (—) vs. mammogram P2 (—)

eight mammograms from the set provided above. We used two patterns for training data and two others for testing data. Figures 7, 8 and 9 show the pdfs of the patterns indicated. The combinations shown were chosen simply for illustrative purposes. In all cases, the ability to discriminate exists and the discriminant boundaries generalize from training to testing data. If these results can be extended to non-malignant abnormal tissue the technique might be useful in distinguishing these types.

Mammograms and Change Point Analysis

The results to be discussed next involve six patients followed for 3 years in which a biopsy proven anomaly was detected in the 3rd year in three of the patients. We used at least two views of each breast for each patient for each year for a total of 81 images. The images were digitized at 600 dpi (approximately 42.3 μm) and 8 bit grayscale. The images were provided by Kaiser-Permanente Research, Portland, Oregon.

We show pictures from only one patient. As will be discussed, we were able to detect an anomaly in the 2nd year. We were not able to do this for the other two cases. However, it may be possible that this technique can result in earlier detection in some cases. We did not detect any false-positives in the other three cases.

Figure 10 shows an image in (a), a grid in (b) showing the subregions, and in (c) the KL surface, KL $(\hat{\alpha}_{ref}, \hat{\alpha}_{i,j})$, for a reference healthy tissue tile against the other tiles i, j. As mentioned, this image is from the 2nd year.

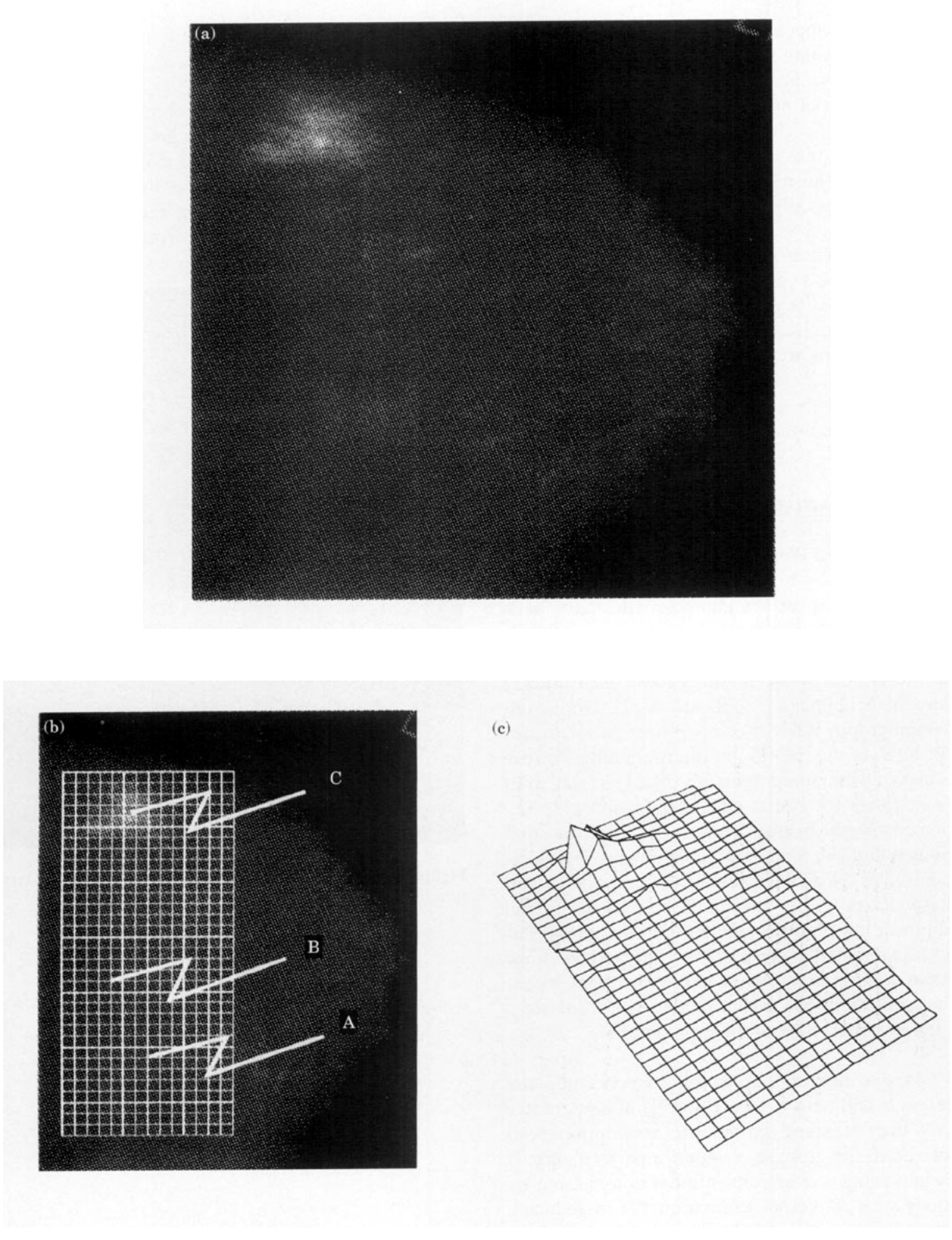

Figure 10. Mammographic change point analysis. (a) A mammogram from year 2. This patient had a tumour detected in the third year of the study. (b) The mammogram from (a) with the grid overlayed. Observations are drawn from each grid tile. Tile A is healthy tissue used as the reference tile. Tile B is another healthy tile. Tile C is in the anomalous region. (c) Kullback-Leibler (KL) surface for the grid shown in (b). The region of large KL values corresponds to the area in which the tumour was detected the following year.

The KL surface appears to be quite homogeneous except at the top where the tumour was detected in the 3rd year. The KL values are significantly greater here, indicating a region of anomalous tissue.

The pdfs from tiles in the healthy region exhibit similar pdfs while those in the anomalous region have a shifted mean and a rather heavier tail.

If histograms of the KL values are constructed for this patient over the 3 years, an estimate of a τ value can be made. Using the 1st year as a baseline healthy set, a $\tau = 2.83$ (maximum KL value) is obtained. For the 2nd year, four detections are obtained, that is, T exceeded τ for four tiles ($T_{max} > 4.5$). For year 3 the number of detections was much greater ($T_{max} = 13.67$) which clearly shows the non-homogeneity detected.

Performance Discussion

Related and Current Work

Breast parenchymal texture characteristics have been studied for their relationship to breast cancer risk (19, 20). Furthermore, texture features have been utilized for many medical imaging applications (21–26) including mammography (27, 28) and power law features have proven to be useful in discriminating texture classes in X-ray mammography (13, 29–31) as well as in other modalities for breast cancer detection (32, 33). The present work begins from the conjecture that suspicious regions in mammographic images will manifest themselves as distinguishable texture classes and that these classes will be distinguishable by the fractal related power law features. While we do not intend this work to be a detailed analysis of the utility of power law features as compared to other texture measures, recent work has indicated that fractal related measures are a viable texture characterization approach (34).

The adaptive mixtures approach to estimating the parameters θ and π in $\hat{\alpha}$ (see Eqn [2]) allows greater flexibility than standard parametric assumptions and therefore holds the promise of superior performance. It also has advantages over conventional non-parametric techniques such as kernel estimation (9) in reducing computational complexity. The potential diagnostic value of the subpopulation groupings provided by the resultant mixture estimator may also be useful. As stated above, the utilization of these probability density estimates for the low-level texture-based information is investigated using discriminant analysis and change point analysis.

The performance of the combination of fractal dimension features utilizing segmentation boundaries and pdfs was analysed (9). The mammogram shown in Figure 11 has a boxed region containing a tumorous region (biopsy verified) with the radiologist's boundary drawn in. The tumorous region (region 1) is the region

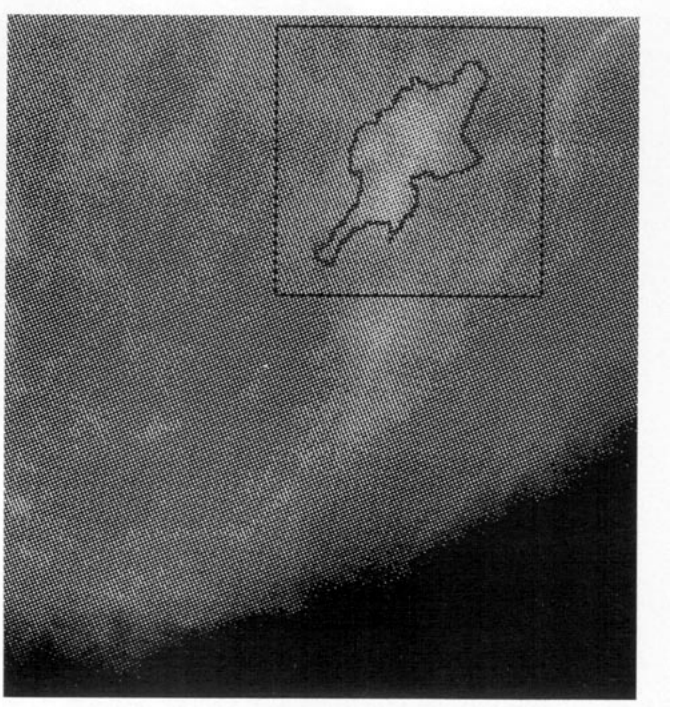

Figure 11. Mammogram with radiologist's boundary of tumorous region overlaid.

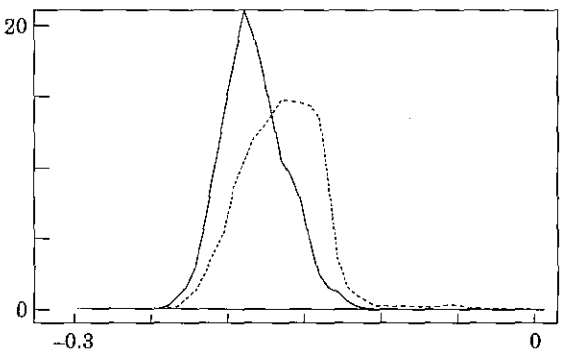

Figure 12. Probability density functions for fractal dimension from Figure 11, calculated using the radiologist's boundary. (——) Tumorous tissue; (-----), healthy tissue.

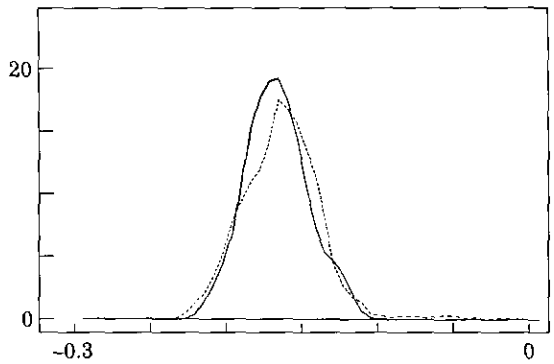

Figure 13. Probability density functions for fractal dimension from Figure 11, calculated with no boundary information. (—), Tumorous tissue; (-----), healthy tissue.

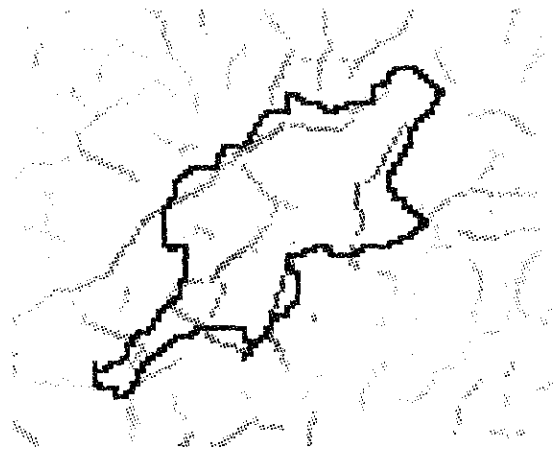

Figure 14. Incomplete, grayscale wavelet segmentation map with radiologist's boundary overlaid. This continuous valued map is used for Figure 15.

within the radiologist's boundary and the healthy region (region 2) is the area simultaneously within the box and outside the tumorous region.

Figures 12 and 13 show, respectively, pdfs for the two regions when the true boundary has been incorporated into the calculation of the features (Figure 12) and when no boundary is used (Figure 13). We clearly see that the presence of the boundary in the feature extraction is vital to the utility of the features for distinguishing tumorous tissue from healthy tissue.

Unfortunately, obtaining a true boundary like that shown in Figure 11 and used in Figure 12 is costly and time-consuming. Furthermore, the ultimate utility of this procedure for a real application depends on the ability to generate a boundary automatically that will

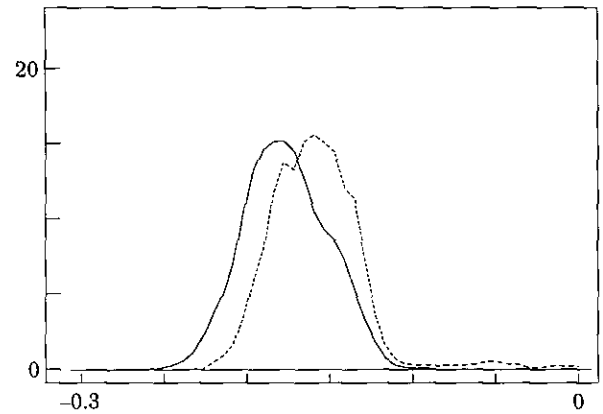

Figure 15. Probability density functions for fractal dimension from Figure 11, calculated using the continuous valued wavelet boundary from Figure 14. (—), Tumorous tissue; (-----), healthy tissue.

be useful in this context. Figure 14 shows the radiologist's boundary superimposed on a particular wavelet segmentation map. This wavelet map is by no means perfect. The boundary is not closed, it is not necessarily exactly coincident with the radiologist's boundary, it is continuously valued rather than binary, and there is noise. Nevertheless, it generally marks the edge of the tumorous region. When this boundary is used in the feature extraction the resultant pdfs are as depicted in Figure 15. We see that the separation of the two classes is maintained to a degree similar to that obtained when the radiologist's boundary was employed. Discriminant analysis could be successfully pursued here, as in Figure 12, while Figure 13 (the no boundary case) leaves little hope.

Future Efforts

The results presented here are preliminary in nature. In fact, few studies if any, have been performed on automated digital mammography processing which are of a large enough scale to draw conclusions about the underlying statistical procedures as opposed to the performance of a system as a whole. The study most closely related to the work presented here is by Caldwell *et al* (29) but the slant of the paper is significantly different than ours. The studies and other related papers by the University of Chicago group (35,36) investigate radiologist performance using computer-aided technology but no comparison can be made on the statistical performance of the integral pieces for such a system.

In our opinion, a comprehensive study of the individual processes described here, in the framework of a computer-aided system is a necessary, albeit complex, next step. The performance of the individual processes cannot be evaluated in a vacuum as there are currently few, if any, useful metrics applicable to the individual processes as opposed to an omnibus computer-aided system.

References

1. Wegman, E.J. (1988) Computational statistics: A new agenda for statistical theory and practice. *J. Wash. Acad. Sci.* **78**:310–322.
2. Mandelbrot, B. (1977) *The Fractal Geometry of Nature.* New York: W.H. Freeman & Co.
3. Solka, J.L., Priebe, C.E. & Rogers, G.W. (1992) An initial assessment of discriminant surface complexity for power law feature. *Simulation* **58**:311–318.
4. Priebe, C.E. & Marchette, D.J. (1991) Adaptive mixture: recursive nonparametric pattern recognition. *Pattern Recognition* **24**:1197–1209.
5. Priebe, C.E. & Marchette, D.J. (1993) Adaptive mixture density estimation. *Pattern Recognition* **26**:771–785.
6. Priebe, C.E. (1994) Adaptive mixtures. *J Statist. Assoc.* **89**:796–806.
7. Silverman, B.W. (1986) *Density Estimation.* New York: Chapman and Hall.
8. Titterington, D.M., Smith, A.F.M. & Makov, U.E. (1985) *Statistical Analysis of Finite Mixture Distributions.* New York: John Wiley and Sons.
9. Priebe, C.E., Julin, E.G., Rogers, G.W., Healy, D.M., Lu, J., Solka, J.L. & Marchette, D.J. (1994) Incorporating segmentation boundaries into the calculation of fractal dimension features. *Proc 26th Symposium on the Interface*, Research Triangle Park, NC.
10. Brodatz, P. (1966) *Texture: A Photographic Album for Artists and Designers.* New York: Dover.
11. Scott, D.W. (1992) *Multivariate Density Estimation* New York: John Wiley and Sons.
12. Duda, R.O. & Hart, P.E. *Pattern Classification and Scene Analysis.* New York: John Wiley and Sons.
13. Priebe, C.E., Solka, J.L., Lorey, R.A., Rogers, G.W., Poston, W.L., Kallergi, M., Qian, W., Clarke, L.P. & Clark, R.A. (1994) The application of fractal analysis to mammographic tissue classification. *Cancer Lett.* **77**:183–189.
14. Priebe, C.E., Solka, J.L. & Rogers, G.W. (1993) Discriminant analysis in aerial images using fractal based features. *Proc. SPIE.* **1962**:196–208.
15. McLachlan, G.J. (1992) *Discriminant Analysis and Statistical Pattern Recognition.* New York: John Wiley and Sons.
16. Priebe, C.E., Lorey, R.A., Marchette, D.J., Solka, J.L. & Rogers, G.W. (1994). Nonparametric spatio-temporal change point analysis for early detection in mammography. *Proc. 2nd Intl. Workshop on Digital Mammography (SIWDM)*, York, UK.
17. Ripley, B.D. (1988) *Statistical Inference for Spatial Processes.* Cambridge: Cambridge University Press.
18. Rogers, G.W., Priebe, C.E., Solka, J.L., Lorey, R.A. & Julin, E.G. (1994) A system and method for incorporating segmentation boundaries into the calculation of fractal dimension for texture discrimination. Patent Application, Navy Case No. 75,998.
19. Wolfe, J.N. (1976) Breast patterns as an index of risk for developing breast cancer. *Am. J. Radiol.* **126**:1130–1139.
20. Saftlas, A.F. & Szklo, M. (1987) Mammographic parenchymal patterns and breast cancer risk. *Epidemiol. Rev.* **9**:146–174.
21. Barnsley, M.F., Massopust, P., Strickland, H. & Sloan, A.D. (1987) Fractal modeling of biological structures. *Ann. NY Acad. Sci.* **504**:179–194.
22. Wu, C-M., Chen, Y.-C. & Hsieh, K.-S. (1992) Texture features for classification of ultrasonic liver images. *IEEE Trans. Med. Imag.* **11**:141–152.
23. Liang, Z., Jaszczak, R.J. & Coleman, R.E. (1992) Parameter estimation of finite mixtures using the EM algorithm and information criteria with application to medical image processing. *IEEE Trans. Nuclear Science.* **39**:1126–1133.
24. Cargill, E.B., Barrett, H.H., Fiete, R.D., Ker, M., Patton, D.D. & Seeley, G.W. (1988) Fractal physiology and nuclear medicine scans. *Proc. SPIE* **914**:355–361.
25. Cargill, E.B., Donoho, K., Kolodny, G., Parker J.A. & Zimmerman, R.E. (1989) Analysis of lung scans using fractals. *Proc. SPIE* **1092**:2–9.
26. Dellepiane, S., Serpico, S.B., Vernazza, G. & Viviani, R. (1987) Fractal-based image analysis in radiological applications. *Proc. SPIE* **845**:396–403.
27. Kimme-Smith, C., Frankl, G., Wassel, G.N. & Sklansky, J. (1979) Toward reliable measurement of breast parenchymal pattern. *Proc. Conf. on Comput. Appl. in Radiol. & Comput./Aided Anal. of Radiol. Images* pp. 118–121.
28. Miller, P. & Astley, S. (1992) Classification of breast tissue by texture analysis. *Image and Vision Comput.* **10**:277–282.
29. Caldwell, C.B., Stapleton, S.J., Holdsworth, D.W., Jong, R.A., Weiser, W.J., Cooke, G. & Yaffe, M.J. (1990) Characteristics of mammographic parenchymal pattern by fractal dimension. *Phys. Med. Biol.* **35**:235–247.
30. Magnin, I.E., Cluzeau, F., Odet, C.L. & Bremond, A. (1986) Mammographic texture analysis: an evaluation of risk for developing breast cancer. *Optical Engineering* **25**:780–784.
31. Liu, X., Zhang, G. & Fox, M.D. (1991) Fractal description and classification of breast tumors. *Proc. Annual Conf. on Eng. in Med. and Biol.* pp. 112–113.
32. Goldberg, V., Manduca, A., Ewert, D.L., Gisvold, J.J. & Greenleaf, J.F. (1992) Improvements in specificity of ultrasonography for diagnosis of breast tumors by means of artificial intelligence. *Medical Physics* **19**:1475–1481.
33. Bronskill, M.J., Yaffe, M.J., Boyd, N.F., Poon, C. & Byng, J. (1991) Correlation of quantitative MRI parameters with mammographic pattern: risk of breast cancer. *Proc. Annual Conf. on Eng. in Med. and Biol.* pp. 108–109.
34. Ohanian, P.P. & Dubes, R.C. (1992) Performance evaluation for four classes of textural features. *Pattern Recognition* **25**:819–833.
35. Astley, S.M. & Taylor, C.J. (1990) Combining cues for mammographic abnormalities. *Proc. BMVC90* pp. 253–258.
36. Chan, H.P., Doi, K., Vyborny, C.J., Schmidt, R.A., Metz, C.E., Lam, K.L., Ogura, T., Wu, Y.Z. & Macmahon, H. Improvement in radiologist's detection of clustered microcalcifications on mammograms. The potential of computer-diagnosis. *Invest. Radiol.* **25**:1102–1110.